RSC Advances

PAPER

View Article Online
View Journal | View Issue

Cite this: *RSC Adv.*, 2015, **5**, 58832

Intense red emitting monoclinic $LaPO_4:Eu^{3+}$ nanoparticles: host–dopant energy transfer dynamics and photoluminescence properties

Santosh K. Gupta,*[a] P. S. Ghosh,[b] M. Sahu,[c] K. Bhattacharyya,[d] R. Tewari[b] and V. Natarajan[a]

$LaPO_4$ nanoparticles were synthesized using complex polymerization method and characterized systematically using X-ray diffraction (XRD), transmission electron microscopy (TEM) and photoluminescence (PL) spectroscopy. Varied concentration of europium ion is doped in the $LaPO_4$ lattice and optical properties and Judd–Ofelt analysis were investigated. It is observed that $LaPO_4$ nanoparticles give violet–blue emission when irradiated with UV light. On doping europium ion the band gap of $LaPO_4$ decreases. Based on DFT calculations it is proposed that energy range over which d and f states of Eu are distributed is coincident with the valence band of $LaPO_4$ so causing an efficient energy transfer from $LaPO_4$ to europium ion. The actual site symmetry for europium ion in lanthanum orthophosphate was also evaluated as D_{2d} based on the Stark splitting pattern although it is C_1 for La^{3+} in $LaPO_4$. The critical energy-transfer distance for the Eu^{3+} ions was evaluated, based on which the quenching mechanism was verified to be an electric multipolar interaction. It is also observed that the red emission intensity of $LaPO_4:Eu^{3+}$ (2.0 mol%) is almost 85% of a commercial red phosphor, which clearly demonstrates that the as-prepared samples are promising red phosphors under near-UV for use in white-light emitting diodes.

Received 15th May 2015
Accepted 18th June 2015

DOI: 10.1039/c5ra09076h

www.rsc.org/advances

1. Introduction

Lanthanide ion doped inorganic materials have attracted significant amount of attention in all areas of science and technology because of their interesting physico-chemical properties and potential applications in many new areas such as drug carriers,[1] telecommunication,[2] photovoltaics and photocatalysis,[3] white light application,[4] contrast agents for MRI and fluorescence imaging,[5] nanothermometry[6] *etc.*

Inorganic compounds bearing f^0, f^7 or f^{14} lanthanide ions have a negligible chance of undergoing quenching effect through cross relaxation from Ln^{3+} ion and hence they are the preferred choice as a host material.[7] In that context $LaPO_4$ is good luminescence host. Also because of its other desirable properties such as low toxicity, environmental stability, ability to accommodate large lanthanide ions, high refractive index and high thermal and chemical stability, it is extensively used as a host matrix.[8,9] In fact, $LaPO_4$ doped with cerium and terbium ion,[10] has been a commercially applied green phosphor in fluorescent lamps. Lanthanum orthophosphate has three different polymorphs; hexagonal, monoclinic and tetragonal. Because the tetragonal phase is stable at high temperature and the hexagonal phase is stable at low temperature, they are not preferred choices for a luminescence host matrix, and it is the monoclinic form which is mainly explored for lanthanide-based photoluminescence (PL). Monoclinic $LaPO_4$ has monazite structure; where lanthanum atoms have nine-fold coordination (LaO_9). It is reported that out of nine bonds; four of the oxygen atoms are oriented in a distorted tetrahedron (PO_4) that interpenetrates a planar pentagon formed by the other five other oxygen atoms.[8] Europium (Eu^{3+}) ions are notable among lanthanides for their characteristic red emission, which is most often excited by ultraviolet (UV) light. Eu^{3+} is also a special ion as it gives symmetry-sensitive emission because of the non-degenerate ground state $^7F_0$ and non-overlapping $^{2S+1}L_J$ multiplets and the most intense transition originates from the $^5D_0$ state which is not split into sublevels due to the crystal field. Furthermore, in a crystal site with inversion symmetry the electric dipole transitions (EDT) are strictly forbidden and the magnetic dipole transitions (MDT) are usually the most intense emission peaks, while for a site without inversion symmetry EDT is usually the strongest emission line, because $\Delta J = \pm 2$ transitions are hypersensitive to small deviation from inversion symmetry. Eu^{3+} is a preferred structural probe and is used extensively for obtaining information about local symmetry, site occupancy *etc.*[11–17]

[a]*Radiochemistry Division, Bhabha Atomic Research Centre, Mumbai 400085, India. E-mail: santufrnd@gmail.com; Fax: +91-22-25505151; Tel: +91-22-25590636*
[b]*Materials Science Division, Bhabha Atomic Research Centre, Mumbai 400085, India*
[c]*Radioanalytical Chemistry Division, Bhabha Atomic Research Centre, Mumbai 400085, India*
[d]*Chemistry Division, Bhabha Atomic Research Centre, Mumbai 400085, India*

Substantial literature reports relate to the optical properties of europium-doped $LaPO_4$. Chen *et al.*[8] have investigated the effect of europium doping on the morphology and optical properties of $LaPO_4$ crystal with varied dopant concentrations whereas Wang *et al.*[18] has studied the influence of phosphate precursor on the PL properties of $LaPO_4$:Eu nanoparticles. Another group[19] has studied the influences of surfactants on PL properties of $LaPO_4$:Eu nanoparticles. Yang *et al.* have studied the effects of the method of synthesis on the characteristics of the $LaPO_4$:Eu phosphors.[20] Another report on the optical properties of europium-doped $LaPO_4$ nanorods and nanoparticles also exists in the literature.[21] Lei *et al.*[22] have explored the effect of lithium ion co-doping on the PL properties of $LaPO_4$:Eu. There are also further reports on the PL properties of Eu^{3+}-doped $LaPO_4$.[23–25]

The most general method of synthesizing a phosphor material is doping different lanthanide ion into suitable inorganic hosts depending on the requirements. But in some cases even without doping any activator ion; hosts show intense self activated emission and subsequently can transfer their excitation energy to activator ions when doped. Therefore, energy transfer from dopant to host has become an effective route to enhance the emission intensity of activators. Some of the recent reports on application of host–dopant energy transfer, where defects play a prominent role, are in NIR phosphorescent phosphors[26] and in deep tissue and cell imaging studies.[27–29]

None of these previous studies discuss about the origin of the violet-blue emission in lanthanum phosphate nanoparticles or explained the energy transfer mechanism on europium doping. Moreover none of these studies discuss about the local site symmetry around Eu^{3+} ion in $LaPO_4$ and covalency of Eu–O bonds as a function of Eu^{3+} concentration.

Doping, which forms the basis of most photonic applications, is best achieved through a wet chemical method such as sol–gel, combustion, use of citrate precursor, microemulsion method. We have employed a citrate precursor route for the synthesis of $LaPO_4$. This citrate precursor method scores over other methods because it is a relatively simple, easy and low-cost technique employing common chemicals with good stoichiometric and particle size control.

In this work we have presented a combined experimental and theoretical study on the optical properties of $La_{1-x}Eu_xPO_4$. Polymeric precursor derived $La_{1-x}Eu_xPO_4$ are characterized by X-ray diffraction (XRD), photoluminescence spectroscopy (PL) and ultraviolet–visible absorption analysis (UV-Vis). An effort was made to correlate the experimental and theoretical results for host–dopant energy transfer. We have studied the effect of europium ion concentration on photoluminescence properties and optical absorption spectroscopy of $La_{1-x}Eu_xPO_4$. We have also investigated the spectroscopic properties of $La_{1-x}Eu_xPO_4$ using Judd–Ofelt theory based on photoluminescence emission spectra as a function of Eu^{3+} concentration.

2. Experimental

2.1. Synthesis

$La_{1-x}Eu_xPO_4$ samples (x = 0, 0.005, 0.01, 0.02 and 0.05) were synthesized by a polymeric precursor route. The starting materials were $(NH_4)_2HPO_4$ (99.99%, M/s Alfa Aesar, Lancaster), La_2O_3 (99.995%, Rare-earth development division, BARC, Mumbai) and Eu_2O_3 (99.999% purity supplied by Aldrich, USA). Citric acid (99.7%, M/s Chemco fine chemicals, Mumbai) was used as the complexing agent while ethylene glycol (99.0%, M/s Thomas Baker, Mumbai) was used for polyesterification to stabilize the complex. Initially the reactants La_2O_3 and Eu_2O_3 were preheated in a highly pure argon atmosphere at 1000 °C to remove moisture. Thereafter La_2O_3 was dissolved in concentrated HNO_3 followed by addition of citric acid. Citric acid was added to maintain the fuel to oxidant ratio as unity. The solution was kept on the hot plate at 80 °C and the required amount of $(NH_4)_2HPO_4$ was added. Ethylene glycol was then added and the mixture stirred. The citric acid and ethylene glycol were added in the mass ratio of 6 : 4. The solution was kept overnight for stable polyester formation. For the Eu-doped samples, the required amount of Eu_2O_3 was also added in the nitric acid dissolution step. Upon evaporation of the reaction solution a transparent polymeric gel was formed. The gel was then burned at 500 °C in a preheated furnace for 1 h. The obtained foamy carbonaceous precursor was then ground, pelletised and kept at 800 °C for 6 h.

2.2. Instrumentation

X-Ray diffraction (XRD) patterns of the powdered undoped and europium-doped $LaPO_4$ samples were recorded using a RIGAKU Miniflex-600 diffractometer operating in Bragg–Brentano focusing geometry. Cu-Kα radiation (λ = 1.5406 Å) was used as the X-ray source and the operating voltage and current of the instrument was kept at 40 kV and 30 mA, respectively. The XRD patterns were collected with scan rate of 1° min^{-1}. PL data were recorded on an Edinburgh CD-920 unit equipped with M 300 monochromators. The data acquisition and analysis were done by F-900 software provided by Edinburgh Analytical Instruments, UK. A xenon flash lamp with frequency range of 10–100 Hz was used as the excitation source. Emission spectra for samples were recorded with a lamp frequency of 100 Hz. Multiple scans (at least five) were taken to minimize the fluctuations in peak intensity and to maximize S/N ratio. Fluorescence lifetime measurements were based on well established time-correlated single-photon counting (TCSPC) technique. Samples for TEM were prepared by suspending particles in a non-aqueous medium. To ensure uniform distribution samples were subjected to ultrasonication for 20 min and a few drops from the liquid were allowed to settle on 200 micron carbon coated copper grids. The grids were allowed to dry under vacuum for a few hours prior to loading in a transmission electron microscope (TEM). A Technai T-20 instrument of FEI was used for all TEM investigation. EPR spectra were recorded on a Bruker ESP-300 spectrometer operating at X-band microwave frequency (9.4186 GHz). Diphenyl picrylhydrazyl (DPPH) was used for the calibration of g-values of paramagnetic species. UV-Vis diffuse reflectance spectra (UV-Vis DRS) of the samples were obtained on an UV-Vis spectrophotometer (Hitachi U-3010) using $BaSO_4$ as reference.

2.3. Computational methodology

All calculations in this study are based on density functional theory (DFT) in conjunction with projector augmented wave

(PAW) potentials, which is implemented in the plane wave based Vienna Ab initio Simulation Package (VASP).[30,31] The generalized gradient approximation (GGA) parameterized by Perdew–Burke–Ernzerhof (PBE)[32] was used as the exchange–correlation functional. The projector augmented wave (PAW) potentials[33] were used for the ion–electron interactions including the valence states of La (5s, 5p, 5f – 11 valence electrons), P (3s, 3p – 5 valence electrons), Eu^{3+} (5p, 6s, 5d – 9 valence electrons) and O (2s, 2p – 6 valence electrons). In our calculations, the Kohn–Sham single-particle wave functions were expanded in a plane-wave basis with kinetic energy cutoff of 500 eV and it was shown that the results were well converged at this cut off. For monoclinic $LaPO_4$ structure, optimization was carried out with respect to plane-wave cut-off energy and *k*-point meshes to ensure convergence of total energy to within a precision of 0.1 meV per atom. In order to study Eu^{3+}-doped systems, a $2 \times 2 \times 1$ supercell of $LaPO_4$ unit cell containing 96 atoms was constructed. The Brillouin-zone (BZ) integrations were performed on an optimized Monkhorst–Pack[34] *k*-point grid of $10 \times 10 \times 8$ for $LaPO_4$ unit cell and $6 \times 6 \times 8$ for $2 \times 2 \times 1$ supercell. The total energy of $LaPO_4$ and Eu^{3+}-doped $LaPO_4$ were optimized with respect to volume (or lattice parameter, *b*/*a*, *c*/*a* ratio), angle and atomic positions. The structural relaxations (*b*/*a*, *c*/*a* ratio and atomic positions) were performed for each structure using the conjugate gradient algorithm until the residual forces and stress in the equilibrium geometry were of the order of 0.005 eV $Å^{-1}$ and 0.01 GPa, respectively. The final calculation of total electronic energy and density of states (DOS) were performed using the tetrahedron method with Blöchl corrections.[35]

3. Results and discussion

3.1. XRD study

Fig. 1 shows the XRD patterns of as-prepared samples of 0.5, 1.0, 2.0 and 5.0 mol% Eu^{3+}-doped $LaPO_4$ samples along with undoped $LaPO_4$. XRD patterns of samples are in agreement with the monoclinic system of pure $LaPO_4$ (JCPDS no. 84-0600) which reveals that all the products are monazite $LaPO_4$ with monoclinic structure in $P2_1/n$ space group. The XRD patterns shown in Fig. 1 do not show any diffraction peak related to pure oxide phase such as La_2O_3 or Eu_2O_3 phase. The fact that such phases are absent is an indication of a homogeneous solid solution of $LaPO_4$ and Eu^{3+}, which further confirms the occupancy of Eu^{3+} ions in the lattice sites of La^{3+} in $LaPO_4$. Although three different polymorphs of $LaPO_4$ exist – hexagonal, monoclinic and tetragonal, it is the monoclinic polymorph which is mostly used in commercial purposes.

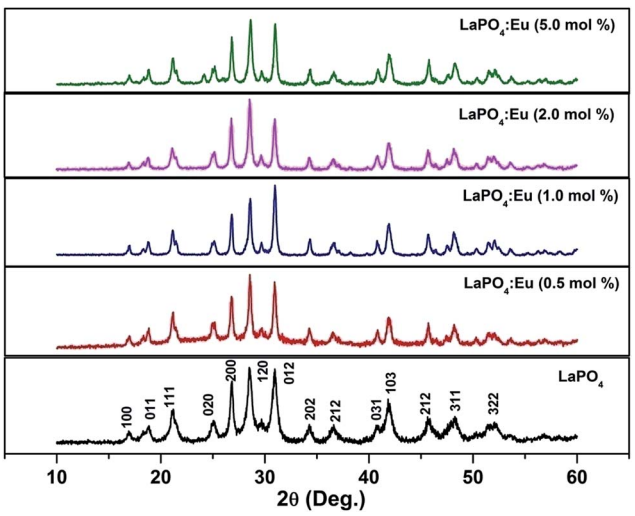

Fig. 1 XRD pattern of undoped and europium-doped $LaPO_4$ samples annealed at 800 °C.

3.2. Transmission electron microscopy (TEM) investigations

Fig. 2 shows a representative TEM micrograph of $LaPO_4$ samples. From the micrograph it can be seen that lanthanum phosphate particles formed are of nano-dimensions with irregular morphology. The average diameter of the $LaPO_4$ particles was found to be approximately 15–30 nm. Selected area electron diffraction (SAED) pattern shows the presence of multiple sharp rings, confirming the nano-dimension and crystalline nature of the particles (inset of Fig. 2). The rings in the patterns could be successfully indexed in terms of the monoclinic phase of $LaPO_4$ which is in agreement with XRD results. The formation of $LaPO_4$ is also confirmed using the EDAX pattern shown in the left inset. The intense copper line arises from the copper-grid used in sample preparation while L and M lines of La and K lines of P and O are also present.

3.3. Luminescence study

Fig. 3 shows the excitation spectra of 0.5 mol% doped Eu^{3+}-doped $LaPO_4$ nanoparticles by monitoring the emission at 593 nm corresponding to the $^5D_0 \rightarrow {}^7F_1$ transition of europium ion. In the spectra a broad band centred at 256 nm is observed which is attributed to a charge transition state (CTS) arising due to transfer of an electron from the filled 2p shell of oxygen to a partially filled 4f shell of Eu^{3+} ion. Fig. 3 (inset) shows a magnified region of 300–450 nm in which the peaks at 322, 364, 384 and 397 nm are observed and correspond to $^7F_{0,1} \rightarrow {}^5H_{3,6}$,

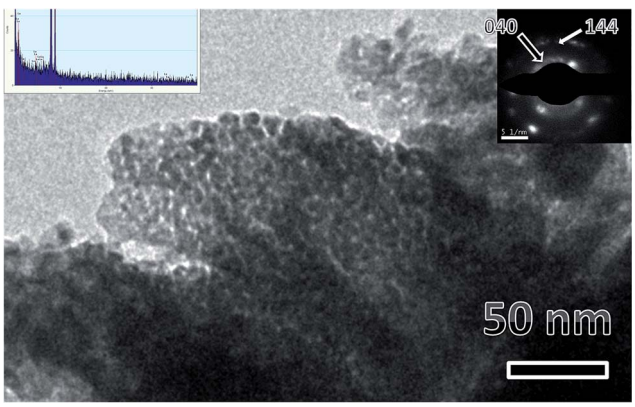

Fig. 2 Representative TEM micrographs of $LaPO_4$ nanoparticles synthesized using the citrate precursor route. Insets are EDS pattern (left top) and selected area electron diffraction (right top).

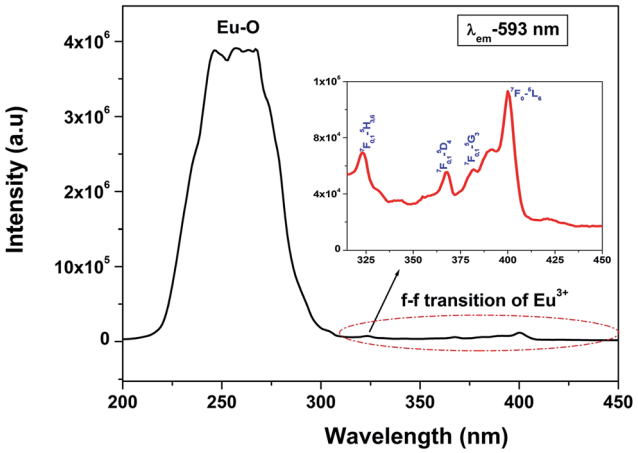

Fig. 3 Excitation spectrum of $LaPO_4$:Eu^{3+} nanoparticles at an emission wavelength of 593 nm.

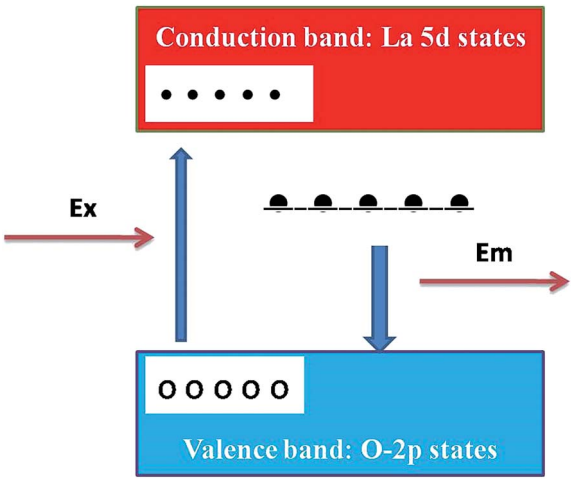

Fig. 5 Schematic model of probable mechanisms responsible for observed emission in $LaPO_4$. In the schematic model, the upper (red) and the lower (light blue) bands are La 5d conduction bands and O 2p valence bands, respectively. The black bar below the conduction band corresponds to the defect level created by the oxygen deficiency. White and black circles correspond to excited holes and electrons, respectively.

$^7F_{0,1} \rightarrow {}^5D_4$, $^7F_{0,1} \rightarrow {}^5G_3$ and $^7F_0 \rightarrow {}^5L_6$ transitions of Eu^{3+}, respectively. These peaks are relatively of weaker intensity compared to the Eu–O charge-transfer band absorption because f → f transitions are of forbidden nature.

Fig. 4a shows the photoluminescent spectrum of undoped $LaPO_4$ nanoparticles with excitation at 230 nm. It consists of a strong broad band in the range of 400–600 nm peaking at 455 nm. Such prominent emission in the case of pure $LaPO_4$ nanoparticles at ~455 nm is also reported by others.[8,36]

The presence of photoluminescence in undoped $LaPO_4$ reveals the presence of defects such as oxygen vacancies, lanthanum interstitials or dangling bonds which can be created during the synthesis procedure. Out of all these, oxygen vacancies are most likely candidate responsible for visible emission in $LaPO_4$. Different types of oxygen vacancies (neutral, singly ionized or doubly ionized) could be responsible for such an intense emission without any activator ion. The presence of oxygen defects, which is responsible for visible emission in $LaPO_4$, is confirmed using EPR. Fig. 4b shows the room-temperature EPR spectrum of $LaPO_4$ which shows an intense peak at $g \sim 1.9684$ which is typical of a singly ionized oxygen vacancy.[37] Such intense violet-blue emission can arise in undoped $LaPO_4$ from transitions of an electron which is formed during photon irradiation near to the conduction band (CB) to single ionized oxygen vacancy centres (V_O^+). Emission in such a case arises from a recombination process wherein an excited electron of the conduction band (CB) loses its energy and re-occupied the energy levels of an electron hole in the valence band (VB) through the localized defect levels. The schematic of defect induced emission is shown in Fig. 5.

Fig. 6 shows the emission spectra of 0.5 mol% Eu^{3+}-doped $LaPO_4$ nanoparticles when excited with 256 nm radiation corresponding to the charge-transfer state. As can be seen, it consists of various sharp lines due to the direct excitation of the Eu^{3+} ions from the ground level to higher levels of the 4f-manifold.

The spectrum consists of main peaks at 593 and 614 nm corresponding to $^5D_0 \rightarrow {}^7F_1$ and $^5D_0 \rightarrow {}^7F_2$ transitions of Eu^{3+}, respectively. Apart from these prominent peaks, we could also observe other weak emission peaks centered at 653 and 697 nm corresponding to $^5D_0 \rightarrow {}^7F_3$ and $^5D_0 \rightarrow {}^7F_4$ transitions, respectively.

The transition $^5D_0 \rightarrow {}^7F_1$ is magnetic dipole (MD) allowed and is not sensitive to the local site symmetry around Eu^{3+} ion.

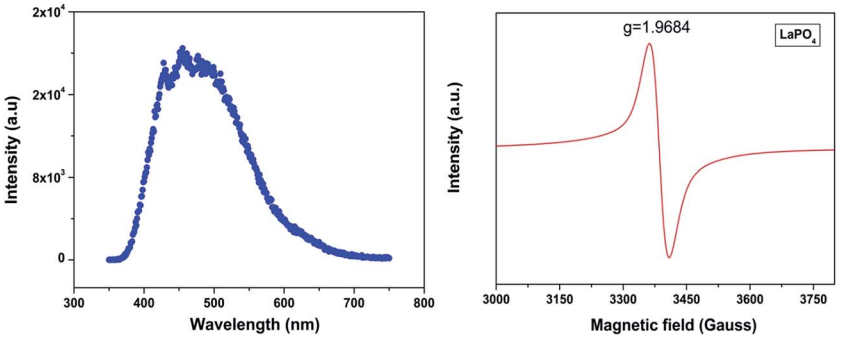

Fig. 4 (a) Emission spectrum of undoped $LaPO_4$ nanoparticles (λ_{ex} – 230 nm) and (b) room-temperature EPR spectra of undoped $LaPO_4$.

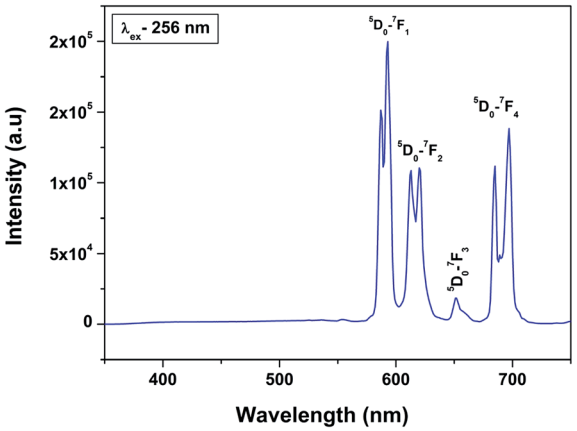

Fig. 6 Emission spectrum of $LaPO_4$:Eu^{3+} (0.5 mol%) at an excitation wavelength of 256 nm.

Transition $^5D_0 \rightarrow {}^7F_1$ is a hypersensitive forced electric dipole (ED) transition and it has electric dipole nature due to the mixing with $4f^{n-1}5d$ states of the opposite parity by the crystal field components. The intensity of this transition is strongly affected by local site symmetry around the Eu^{3+} ions and by the strength of electric field in the Eu^{3+} environment. The other transition $^5D_0$–$^7F_3$ has a mixed ED and MD character while transition $^5D_0$–$^7F_4$ is an ED transition.

The absence of broad host emission due to surface defects in emission spectra of the doped sample indicate incomplete energy transfer at 0.5 mol% of dopant ion concentration.

Among all the transitions observed, the $^5D_0 \rightarrow {}^7F_1$ transition is the strongest and is characterized by an orange–red emission whereas the $^5D_0 \rightarrow {}^7F_2$ transition is characterized by red emission. Generally in a crystal site with inversion symmetry the EDT are strictly forbidden and the MDT are usually the most intense emission peak whereas in a site without inversion symmetry EDT is usually the strongest emission line, because $\Delta J = \pm 2$ transitions are hypersensitive to small deviations from inversion symmetry. A sensitive parameter for understanding symmetry is the asymmetry ratio (I) which is described as ratio of integral intensities of EDT ($^5D_0 \rightarrow {}^7F_2$) to MDT ($^5D_0 \rightarrow {}^7F_1$). The fact that MDT is more intense than EDT (asymmetry ratio is less than unity), indicating that the majority of Eu^{3+} are at sites with inversion symmetry.

When the Eu^{3+} ion is inserted into any chemical/ligand environment (crystal field), the $(2J + 1)$-degenerate J-energy levels get split into the so-called Stark sub-levels by the ligand-field effect with the number of levels depending on the local site symmetry of the metal ion. It is reported that in $LaPO_4$ systems, both La^{3+} as well as phosphate ions occupy C_1 point group symmetry sites.[38] The substitution of La^{3+} with Eu^{3+} may not result in significant lattice distortion because of identical charges, and any distortion would arise only due to size differences (103.2 pm for La^{3+} and 94.7 for Eu^{3+}). From the Stark splitting pattern shown in Fig. 7, two lines for $J = 0 \rightarrow J = 1$ transition, two lines for $J = 0 \rightarrow J = 2$ transition, two lines for $J = 0 \rightarrow J = 3$ transition and four lines for $J = 0 \rightarrow J = 4$ transition of Eu^{3+} were resolved for $LaPO_4$:Eu^{3+} (0.5 mol%). The fact that the $^5D_0 \rightarrow {}^7F_0$ transition is absent rules out the

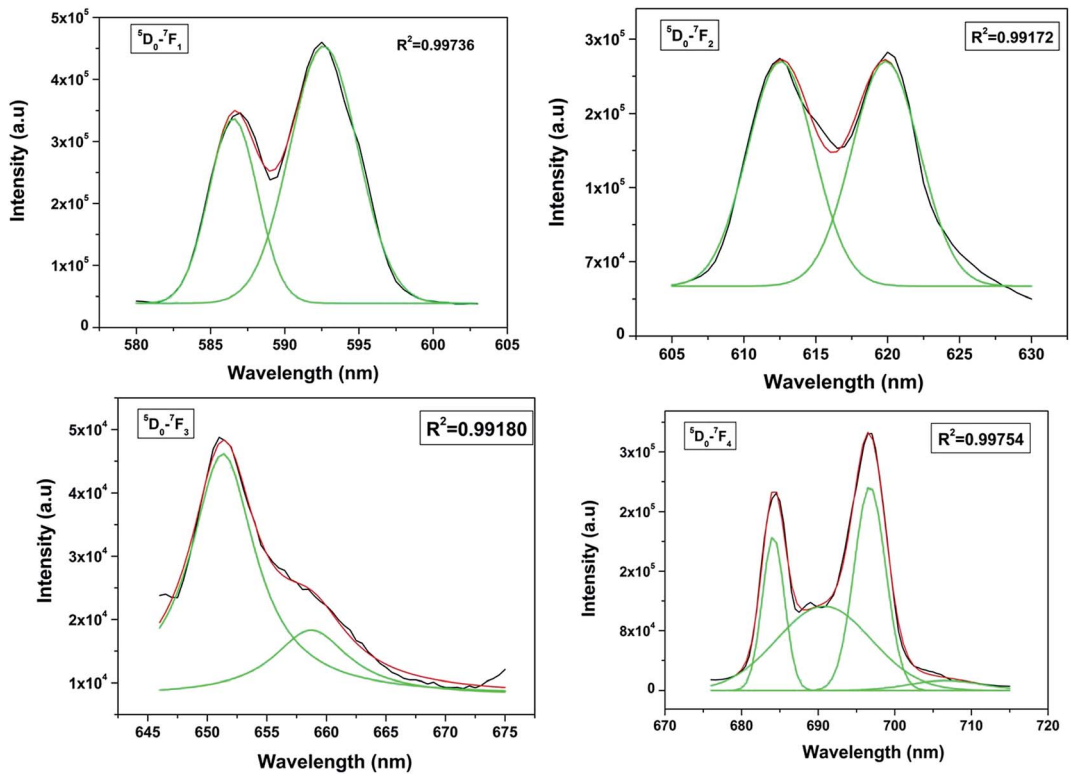

Fig. 7 Stark splitting pattern of europium emission in lanthanum phosphate nanoparticles.

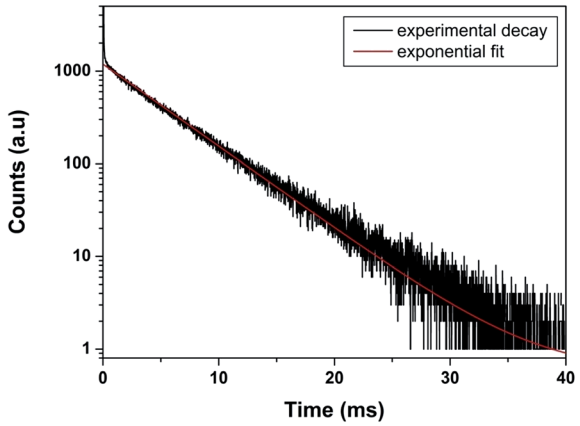

Fig. 8 Photoluminescence decay profile of $LaPO_4:Eu^{3+}$ (0.5 mol%) at emission and excitation wavelength of 593 and 256 nm, respectively.

possibility of the presence of C_{4v} symmetry.[39,40] Therefore the other possibility is D_{2d} site symmetry of Eu^{3+} in $LaPO_4$.

As far as PL decay behavior is concerned, the 0.5 mol% doped sample shows monoexponential behavior (Fig. 8) which indicates that europium ion is uniformly distributed in the $LaPO_4$ host lattice and occupies La^{3+} sites only. The fitting equation is given by eqn (1):

$$I = I_0 + A\exp(-t/\tau) \quad (1)$$

where I is the emission intensity at time t, and A is the initial intensity at $t = 0$. Here, I_0 is a constant, t is time, and τ is the lifetime. The lifetime value obtained in this case is 4.89 ms, which are typically larger than that for most europium-doped phosphor materials, and thus could be a potential material for optical applications.

3.4. Effect of dopant ion concentration on optical properties of $LaPO_4$:Eu

Emission spectra of Eu^{3+} activated $LaPO_4$ phosphors at different Eu^{3+} concentrations with excitation wavelength of 256 nm are shown in Fig. 9. It can be seen that there is not much change in the emission spectral features as a function of Eu^{3+} ion concentration. However, emission intensity increases with increase in Eu^{3+} ion concentration reaching a maximum at 2.0 mol%. Beyond 2.0% the intensity decreases due to concentration quenching, this resulting from resonant energy transfer between Eu^{3+} ions. To have a better understanding of the concentration quenching mechanism, the critical distance (R_c) needs to be evaluated using eqn (2):[41]

$$R_c = 2\left(\frac{3V}{4\pi X_c N}\right)^{\frac{1}{3}} \quad (2)$$

where R_c is the critical distance between the dopant ion and quenching site, V is the volume of the unit cell, X_c is the critical concentration of Eu^{3+} ions, and N is the number of cations per unit cell.

For the $LaPO_4$ host lattice, $V = 304.86$ Å^3, $N = 4$ (four formula units per unit cell), and $X_c = 0.02$. Based on this value the

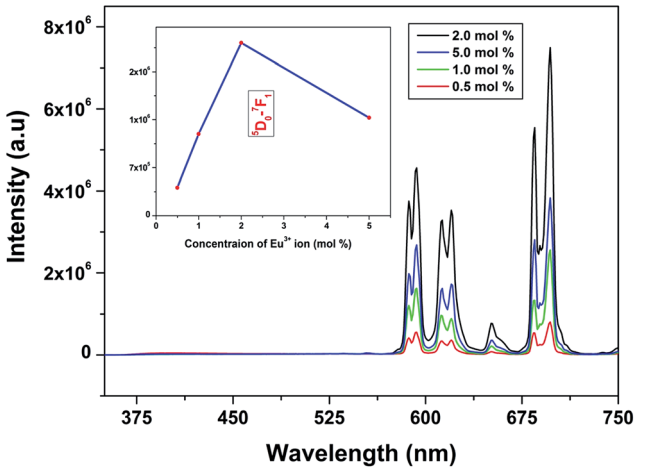

Fig. 9 PL emission spectra (corrected w.r.t. source) of $LaPO_4:Eu^{3+}$ phosphors (mol% of Eu^{3+} = 0.5, 1.0, 2.0, 5.0) excited at 256 nm. The insets show the PL emission intensities of $^5D_0$–$^7F_1$ as a function of Eu^{3+} ion concentration.

critical distance is calculated to be 19.37 Å. In this case, the Eu^{3+}–Eu^{3+} distance is larger than 10 Å. Thus exchange interactions can be ruled out. Therefore, the electric multipolar interaction is believed to be the only mode for the energy transfer among the Eu^{3+} ions in $LaPO_4$ phosphor.

The effect of dopant ion concentration on lifetime value was also investigated and is shown in Fig. 10. It can be seen that all the samples exhibit monoexponential behavior indicating uniform distribution of europium at La^{3+} sites. The lifetime values increase up to 2.0 mol% and beyond that decreases due to concentration quenching. The lifetime values are 4.89, 5.77, 6.23, 6.08 ms for 0.5, 1.0, 2.0, 5.0 mol% europium, respectively. At higher concentration, when the critical distance reaches the value of 19.37 Å, the probability of cross-relaxation between Eu^{3+} becomes very high and thereby reduces the lifetime. There is a close correspondence between the effect of concentration on emission intensity and PL lifetimes.

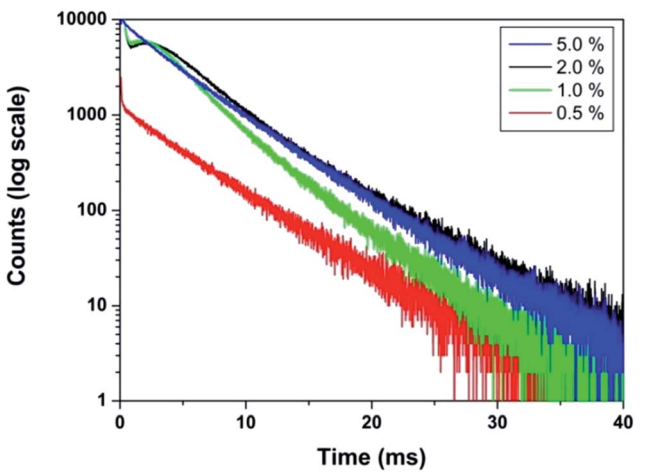

Fig. 10 PL decay curves of $LaPO_4:Eu^{3+}$ samples (Eu^{3+} mol% = 0.5, 1.0, 2.0, 5.0) (monitored at 592 nm and excited at 256 nm).

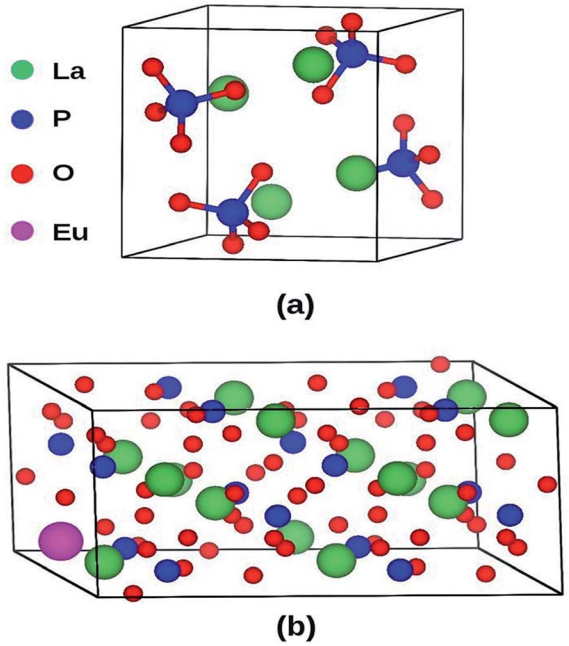

Fig. 11 (a) Unit cell of $LaPO_4$ (24 atoms) and (b) Eu^{3+}-doped 2 × 2 × 1 supercell (96 atoms) of $LaPO_4$.

3.5. Band gap calculations: theory and experiment (DFT and DRS measurements)

$LaPO_4$ has a monoclinic crystal structure ($P2_1/n$ space group, no. 14) having four formula units per unit cell. The PAW-PBE calculated lattice parameters of this phase are $a = 6.9372$ Å, $b = 7.1455$ Å, $c = 6.5411$ Å ($V_0 = 314.98$ Å^3) and $\beta = 103.73°$ ($\alpha = \gamma = 90°$) (Fig. 11) which matches very well with the experimentally determined values, $a = 6.8313$ Å, $b = 7.0705$ Å, $c = 6.5034$ Å and $\beta = 103.27°$.[42] The calculated relaxed atomic positions are compared with experimentally determined atomic positions in Table 1. All the calculated structural parameters of the $LaPO_4$ unit cell are matching within 1.5% of experimentally measured room-temperature values[42] and to within 0.2% of previous GGA calculations.[43]

The PAW-PBE calculated total and angular momentum projected electronic density of states (DOS) of $LaPO_4$ is presented in Fig. 12. From Fig. 12 it can be noted that the

Table 1 Comparison of PAW-PBE calculated and experimentally determined atomic positions

	Atomic positions (this study)			Atomic positions (ref. 42)		
	x	y	z	x	y	z
La (4e)	0.2851	0.1589	0.0988	0.2815	0.1603	0.1006
P (4e)	0.3042	0.1618	0.6109	0.3047	0.1639	0.6121
O1 (4e)	0.2496	0.0064	0.4414	0.2503	0.0077	0.4477
O2 (4e)	0.3811	0.3293	0.4977	0.3799	0.3315	0.4964
O3 (4e)	0.4710	0.1035	0.8042	0.4748	0.1071	0.8018
O4 (4e)	0.1287	0.2129	0.7082	0.1277	0.2168	0.7101

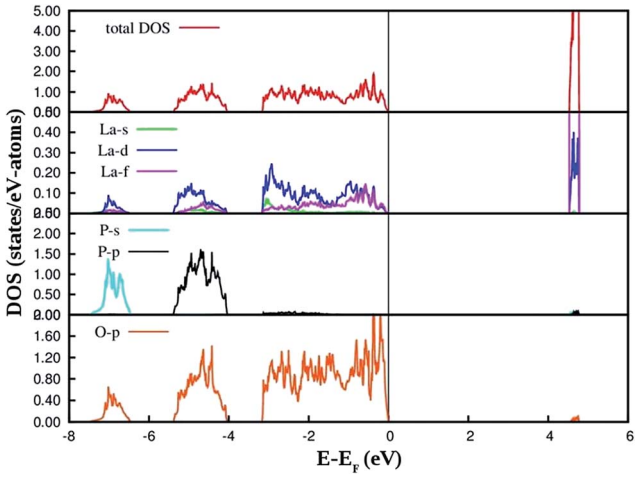

Fig. 12 PAW-PBE calculated total and angular momentum decomposed DOS of $LaPO_4$.

conduction band from 4.5 to 4.8 eV is formed primarily by the La 5d and f states. The valence band is located from −7.5 eV to 0. Besides the small contribution from La s, d and f states, the main contribution of the valence band arises from the O 2p states and P 3s, 3p states due to the strong hybridization effects. It is evident from Fig. 12 that the top of the valence band is formed predominantly by p states of oxygen with admixture of small amounts of La d and f states. The lower part of the valence band is mainly s and p state of P, p states of O along with very small contribution of La d and f states.

The PAW-PBE calculated total and angular momentum projected electronic DOS of Eu^{3+}-doped $LaPO_4$ is presented in Fig. 13. The overall DOS of Eu^{3+}-doped $LaPO_4$ resembles $LaPO_4$ DOS except for the impurity states very near to the Fermi level. The major contribution of Eu atom to the valence band is from d as well as f states and contributions to the conduction band

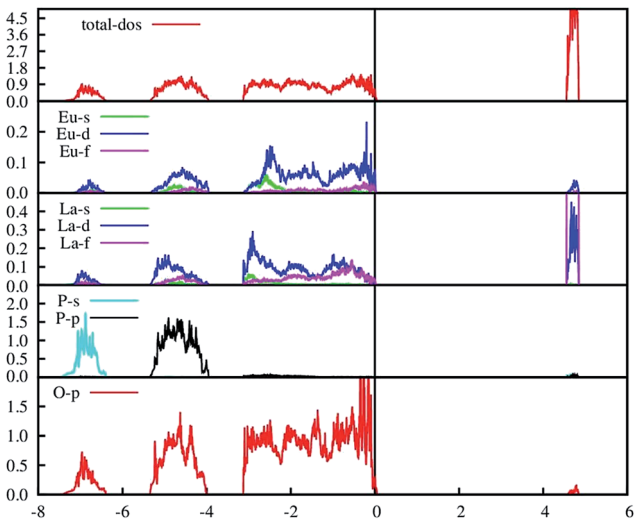

Fig. 13 PAW-PBE calculated total and angular momentum decomposed DOS of Eu^{3+}-doped $LaPO_4$ (doping level is 6.25% at La^{3+} position).

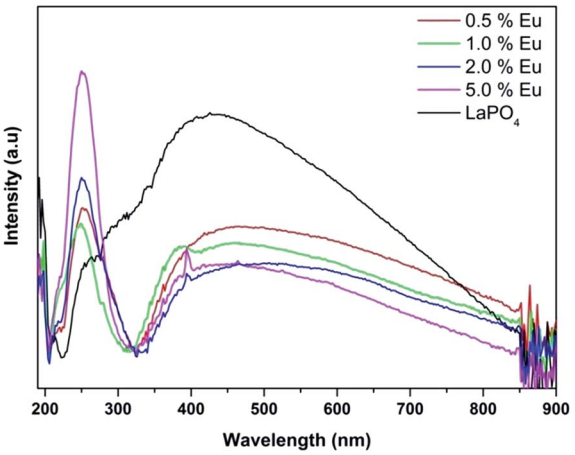

Fig. 14 UV-Vis diffuse reflectance spectra of $LaPO_4$ and $La_{1-x}Eu_xPO_4$.

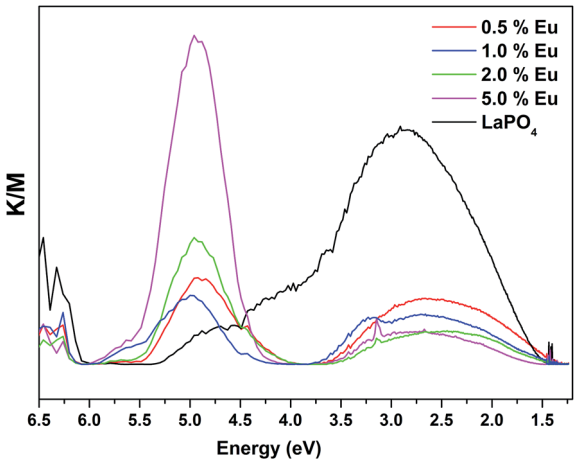

Fig. 15 UV-Vis absorption–energy curves of $LaPO_4$ and $La_{1-x}Eu_xPO_4$.

are from solely Eu d states. Moreover, the energy range over which d and f states of Eu are distributed is exactly coincident with the valence band of $LaPO_4$. Therefore, our DFT study predicts host ($LaPO_4$) to dopant (Eu^{3+}) energy transfer is preferable. Impurity energy states are contributed by Eu d and f states. An impurity state reduces the band gap of Eu^{3+}-doped $LaPO_4$ by ~10% with respect to pure $LaPO_4$.

Fig. 14 and 15 illustrate the UV-Vis absorption spectra and absorption–energy curves (according to the Kubelka–Munk function), respectively, of undoped and europium-doped $LaPO_4$ nanoparticles. It can be seen from the spectra that there is an absorption edge at around 252 nm which appears only on europium doping. Band gap values at different europium concentrations according to the KM spectra are listed in Table 2. It was observed that the band gap value of $LaPO_4$ becomes narrower on europium doping and this phenomenon is known as band gap narrowing (BGN), which is in accordance with DFT calculations, and can be easily seen from Fig. 16. BGN is related to the change in the nature and strength of $LaPO_4$ crystalline potential on europium doping (which has 4f valence electrons) which also influence its electronic level.[44] Upon doping even at a low level of 0.5 mol% the impurity band broadens and merges with the bottom of the conduction band and thereby decreases the band gap of the material. With increase in europium concentration beyond 0.5% there is essentially no further change in band gap value.

Table 2 Calculated band gap for undoped and europium-doped $LaPO_4$

Sample	Band gap/eV
$LaPO_4$	6.15
$LaPO_4$:Eu (0.5 mol%)	4.13
$LaPO_4$:Eu (1.0 mol%)	4.16
$LaPO_4$:Eu (2.0 mol%)	4.25
$LaPO_4$:Eu (5.0 mol%)	4.35

3.6. Judd–Ofelt calculation: photophysical properties

Judd–Ofelt (JO) intensity parameters, Ω_J (J = 2, 4) calculated using Judd–Ofelt theory[45,46] provide information about the local environment in the proximity of lanthanide ion. The application of JO theory to the quantitative analysis of Eu^{3+} emissive properties in a matrix is nicely presented by Werts *et al.*,[47] and also by our group[11,12,48]

Since the $^5D_0 \rightarrow {}^7F_1$ transition, a magnetic dipole transitions is not affected much by environmental effects, its transition rate is constant with an approximate value of 50 s^{-1}.[49] For $LaPO_4$ we have adopted a value for the refractive index of 1.78 for calculation. Emission quantum efficiency of the emitting $^5D_0$ level is written as eqn (3):

$$\eta = \frac{A_R}{A_R + A_{NR}} = \tau \sum_{J=1-4} A_J \quad (3)$$

where the A_R rate was obtained by summing over the radiative rates for each $^5D_0 \rightarrow {}^7F_J$ (J = 1–4). The JO parameter and other photophysical values are listed in Table 3.

It is reported that the Ω_2 parameter is related to the symmetry and the Ω_4 parameter to long-range effects and electronic density surrounding the rare earth ion.[50–52] It was observed that at all concentrations of Eu^{3+} the Ω_4 value is greater than Ω_2 indicating the existence of a symmetric environment around europium ions in $LaPO_4$ which is highly probable because it occupies La^{3+} sites (no charge imbalance). This is also reflected in the intense MDT compared to EDT in our emission spectra. Also D_{2d} point symmetry is observed for europium ion in $LaPO_4$ which is relatively higher symmetry. It can also be seen from Table 3 that the Ω_2 value increases with increase in Eu^{3+} concentration up to 2.0 mol% and thereafter decreases. This reveals that with increase in europium ion concentration the covalency of the M–L bond increases as does the distortion.

The value of Ω_4 is not directly related to symmetry around Eu^{3+} but it does depend on electron density around the ligands. The fact that its value also increases with increase in dopant ion concentration indicates that the electron density on the ligand decreases.

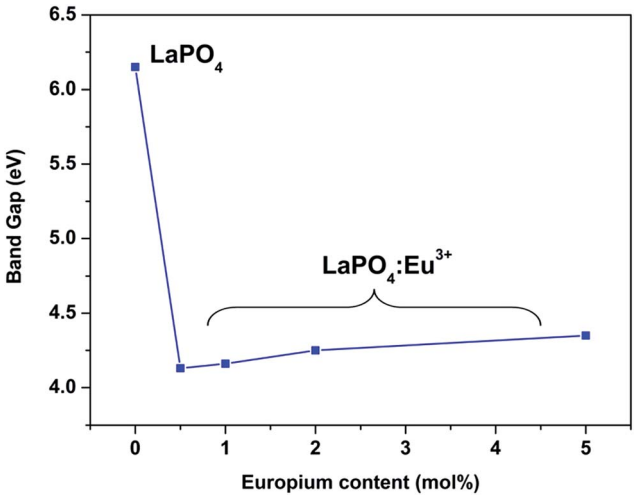

Fig. 16 The energy gap dependence of $LaPO_4$:Eu nanoparticles on the Eu doping level.

Table 3 Photophysical properties Eu^{3+}-doped $LaPO_4$

Eu^{3+} mol%	A_R/s^{-1}	A_{NR}/s^{-1}	η (%)	$\Omega_2/10^{-20}$ cm^2	$\Omega_4/10^{-20}$ cm^2
0.5	179	85	87.7	0.919	3.17
1.0	210	72	88.4	0.962	3.26
2.0	269	63	91.2	1.25	3.72
5.0	234	69	89.3	1.13	3.45

Form Table 3 it can also be seen that, with increase in Eu^{3+} ion concentration up to 2.0 mol% that the radiative transition rate (A_R) increases and non-radiative rate (A_{NR}) decreases. This is matching with our emission spectral data where concentration quenching was observed beyond 2.0 mol% due to cross relaxation between europium ions. The ratio of intensity of electric dipole ($^5D_0 \rightarrow {}^7F_2$) to magnetic dipole ($^5D_0 \rightarrow {}^7F_1$), the asymmetry ratio ($I$) in Eu^{3+}, is related to the degree of covalency between Eu^{3+} and O^{2-}.[53] The larger the difference in the intensities of these two lines, the larger is the asymmetry and covalency effects. For all the samples $^5D_0 \rightarrow {}^7F_1$ is markedly more intense as compared with the $^5D_0 \rightarrow {}^7F_2$ line *i.e.* R/O (red to orange ratio) shows a marked decrease, indicating high symmetry around the Eu^{3+} ion site, as also reflected by the JO parameters.

4. Potential application of Eu^{3+}-doped $LaPO_4$ as a luminescent material

To evaluate the material performance for phosphor applications, CIE chromaticity coordinates were evaluated for the $LaPO_4$:Eu (2.0 mol%) sample adopting standard procedures. This is represented as the point '*' in the CIE diagram shown in Fig. 17. It is clear from the values that $LaPO_4$:Eu shows red emission with very high quantum efficiency of 91.2%. This is because of the fact that non-radiative losses are very low in this particular system. For the application of red phosphors in white

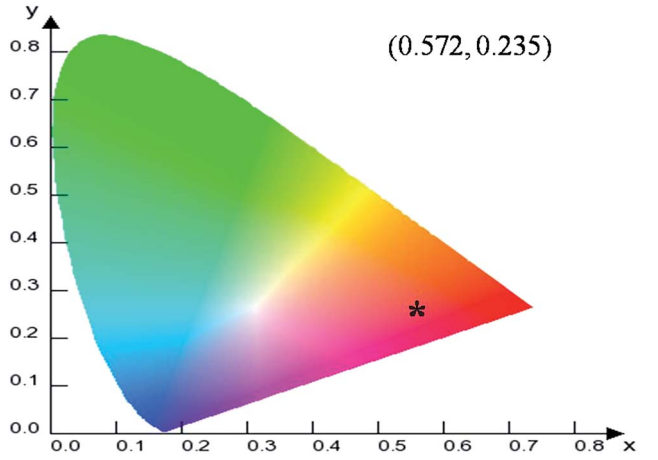

Fig. 17 CIE diagram showing the co-ordinates and representing the color emitted by $LaPO_4$:Eu^{3+}.

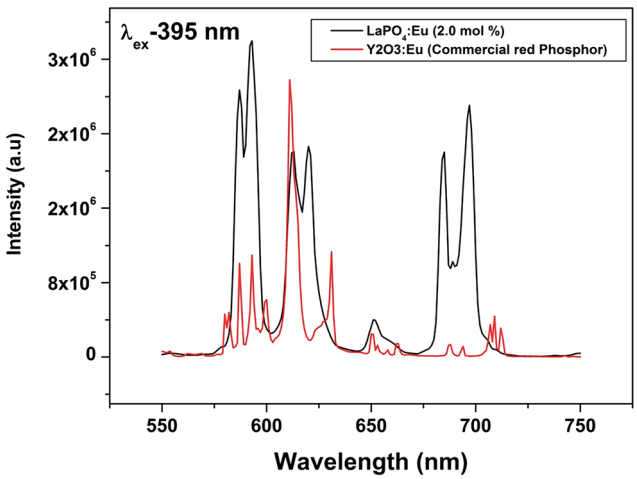

Fig. 18 Comparison of emission spectra of commercial red phosphor (Y_2O_3:Eu from Nichia Corporation, Japan) and $LaPO_4$:Eu^{3+} (2.0 mol%) under 395 nm excitation. The comparison is made on corrected spectra and integral intensity of all the peak is considered.

LEDs with near UV light as the excitation source, the emission spectra of $LaPO_4$:Eu^{3+} (2.0 mol%) and red phosphor (Y_2O_3:Eu from Nichia Corporation, Japan) were compared using the same excitation wavelength of 395 nm (near UV light) (Fig. 18). It is observed that the red emission intensity of $LaPO_4$:Eu^{3+} (2.0 mol%) is almost 85% of the commercial red phosphor, which clearly demonstrates that the as-prepared samples are a promising red phosphor under near-UV radiation for white light emitting diodes.

5. Conclusions

Monoclinic $LaPO_4$ nanoparticles of 20–30 nm size were synthesized using complex polymerization method and characterized systematically using X-ray diffraction (XRD), transmission electron microscopy (TEM) and photoluminescence (PL) spectroscopy. XRD shows the formation of the pure phase

of $LaPO_4$ and europium doping does not distort the crystal structure. The crystallinity and purity of the sample is further studied using EDAX and SAED. Based on PL and EPR it was inferred that intense violet–blue emission in the undoped sample is due to transitions of electrons which are formed during photon irradiation near to the conduction band (CB) to generate single ionized oxygen vacancy centres in $LaPO_4$ nanoparticles. On europium doping, energy is completely transferred from the host to dopant ion, as also predicted using DFT calculations. Europium doping reduces the band gap of $LaPO_4$ by almost 10%. Effects of europium ion on PL intensity, lifetime and photophysical properties were studied extensively. MDT is more intense than EDT in all samples indicating that the majority of Eu^{3+} are at relatively symmetric sites. This is also reflected in the JO parameters; at all concentrations Ω_4 value is greater than Ω_2 indicating the existence of low covalency between Eu^{3+} and ligand and symmetric environment around europium ion in $LaPO_4$, which is highly probable because Eu^{3+} occupies La^{3+} sites (no charge imbalance). The point symmetry of Eu^{3+} in $LaPO_4$ is D_{2d} as calculated using the Stark splitting pattern. It was seen that $LaPO_4$:Eu gives red emission with very high quantum efficiency of 91.2% for a 2.0 mol% doped sample. It is almost comparable to commercial red phosphor in terms of its efficiency indicating its potential for use as a red emitter in future LEDs.

References

1 C. Lv, W. Di, Z. Liu, K. Zheng and W. Qin, *Dalton Trans.*, 2014, **43**, 3681.
2 D. Xu, Y. Zhang, D. Zhang and S. Yang, *CrystEngComm*, 2015, **17**, 1106.
3 W. Yang, X. Li, D. Chi, H. Zhang and X. Liu, *Nanotechnology*, 2014, **25**, 482001.
4 B. Mutelet, S. Boudin, O. Pérez, J. M. Rueff, C. Labbé and P. A. Jaff, *Dalton Trans.*, 2015, **44**, 1186.
5 F. Chen, M. Chen, C. Yang, J. Liu, N. Luo, G. Yang, D. Chen and L. Li, *Phys. Chem. Chem. Phys.*, 2015, **17**, 1189.
6 E. Hemmer, M. Quintanilla, F. Legare and F. Vetrone, *Chem. Mater.*, 2015, **27**, 235.
7 G. Phaomei, R. S. Ningthoujam, W. R. Singh, R. S. Loitongbam, N. S. Singh, A. Rath, R. R. Juluri and R. K. Vatsa, *Dalton Trans.*, 2011, **40**, 11571.
8 H. Chen, Y. Ni, X. Ma and J. Hong, *J. Colloid Interface Sci.*, 2014, **428**, 141.
9 D. Che, X. Zhu, P. Liu, Y. Duan, H. Wang, Q. Zhang and Y. Li, *J. Lumin.*, 2014, **153**, 369.
10 J. Fang, M. Saunders, Y. Guo, G. Lu, C. L. Raston and K. S. Iyer, *Chem. Commun.*, 2010, **46**, 3074.
11 R. Shukla, S. K. Gupta, V. Grover, V. Natarajan and A. K. Tyagi, *Dalton Trans.*, 2015, **44**, 10628.
12 R. Gupta, S. K. Gupta, J. S. Gamre, K. V. Lohithakshan, V. Natarajan and S. K. Aggarwal, *Eur. J. Inorg. Chem.*, 2015, 104.
13 S. K. Gupta, M. K. Bhide, S. V. Godbole and V. Natarajan, *J. Am. Ceram. Soc.*, 2014, **97**, 3694.
14 R. Phatak, S. K. Gupta, K. Krishnan, S. K. Sali, S. V. Godbole and A. Das, *Dalton Trans.*, 2014, **43**, 3306.
15 S. K. Gupta, M. Mohapatra, V. Natarajan and S. V. Godbole, *RSC Adv.*, 2013, **3**, 20046.
16 S. K. Gupta, M. Mohapatra, V. Natarajan and S. V. Godbole, *J. Mater. Sci.*, 2012, **47**, 3504.
17 S. K. Gupta, M. Mohapatra, S. Kaity, V. Natarajan and S. V. Godbole, *J. Lumin.*, 2012, **132**, 1329.
18 X. Z. Wang, *J. Mater. Sci.: Mater. Electron.*, 2014, **25**, 1264.
19 X. Y. Sun, X. D. Sun, X. G. Li, J. He and B. S. Wang, *Nanosci. Nanotechnol. Lett.*, 2014, **6**, 420.
20 S. H. Yang, C. K. Yang, J. H. Yan and C. M. Lin, *J. Electron. Mater.*, 2014, **43**, 3593.
21 P. Ghosh, A. Kar and A. Patra, *J. Appl. Phys.*, 2010, **108**, 113506.
22 W. Lei and J. Lee, *J. Phys. Chem. C*, 2008, **112**, 11679.
23 J. Li, X. Wu, Y. Fan, Y. Li, L. Hu and C. Tang, *Mater. Chem. Phys.*, 2010, **124**, 1172.
24 G. Phaomei, R. S. Ningthoujam, W. R. Singh, N. S. Singh, M. N. Luwang, R. Tewari and R. K. Vatsa, *Opt. Mater.*, 2010, **32**, 616.
25 M. J. Fisher, W. Wang, P. K. Dorhout and E. R. Fisher, *J. Phys. Chem. C*, 2008, **112**, 1901.
26 Y. Li, Y. Li, R. Chen, K. Sharafudeen, S. Zhou, M. Gecevicius, H. Wang, G. Dong, Y. Wu, X. Qin and J. Qiu, *NPG Asia Mater.*, 2015, **7**, e180.
27 Y. Li, S. Zhou, Y. Li, K. Sharafudeen, Z. Ma, G. Dong, M. Peng and J. Qiu, *J. Mater. Chem. C*, 2014, **2**, 2657.
28 Y. Li, Y. Li, K. Sharafudeen, G. Dong, S. Zhou, Z. Ma, M. Peng and J. Qiu, *J. Mater. Chem. C*, 2014, **2**, 2019.
29 Y. Li, S. Zhou, G. Dong, M. Peng, L. Wondraczek and J. Qiu, *Sci. Rep.*, 2013, **4**, 4059.
30 G. Kresse and J. Furthmueller, *Phys. Rev. B: Condens. Matter*, 1996, **54**, 11169.
31 G. Kresse and J. Furthmueller, *Comput. Mater. Sci.*, 1996, **6**, 15.
32 J. P. Perdew, K. Burke and M. Enzerhof, *Phys. Rev. Lett.*, 1996, **77**, 3865.
33 P. E. Blöchl, *Phys. Rev. B: Condens. Matter*, 1994, **50**, 17953.
34 H. J. Monkhorst and J. D. Pack, *Phys. Rev. B: Solid State*, 1976, **13**, 5188.
35 P. E. Blöchl, O. Jepsen and O. K. Andesen, *Phys. Rev. B: Condens. Matter*, 1994, **49**, 16223.
36 N. P. Shaik, N. V. P. Rao and K. V. R. Murthy, *Adv. Mater. Lett.*, 2014, **5**, 722.
37 C. Zhang and J. Lin, *Chem. Soc. Rev.*, 2012, **41**, 7938.
38 A. Hezel and S. D. Ross, *Spectrochim. Acta*, 1966, **22**, 1949.
39 S. V. Eliseevaa and J. C. G. Bunzli, *Chem. Soc. Rev.*, 2010, **39**, 189.
40 Q. Ju, Y. Liu, R. Li, L. Liu, W. Luo and X. Chen, *J. Phys. Chem. C*, 2009, **113**, 2309.
41 G. Blasse, *Phys. Lett. A*, 1968, **28**, 444.
42 Y. X. Ni, J. M. Hughes and A. N. Mariano, *Am. Mineral.*, 1995, **80**, 21.
43 K. Toyoura, N. Hatada, Y. Nose, T. Uda and I. Tanaka, *Phys. Rev. B: Condens. Matter Mater. Phys.*, 2011, **84**, 184301.
44 A. A. Dakhel, *Opt. Mater.*, 2009, **31**, 691.

45 B. R. Judd, *Phys. Rev.*, 1962, **127**, 750.
46 G. S. Ofelt, *J. Chem. Phys.*, 1962, **37**, 511.
47 M. H. V. Werts, R. T. F. Jukes and J. W. Verhoeven, *Phys. Chem. Chem. Phys.*, 2002, **4**, 1542.
48 S. K. Gupta, M. Mohapatra, S. V. Godbole and V. Natarajan, *RSC Adv.*, 2013, **3**, 20046.
49 G. F. de Sa, O. L. Malta, C. M. Donega, A. M. Simas, R. L. Longo, P. A. Santa-Cruz and E. F. da Silva, *Coord. Chem. Rev.*, 2000, **196**, 165.
50 E. M. Rodrigues, E. R. Souza, J. H. S. K. Monteiro, R. D. L. Gaspar, I. O. Mazali and F. A. Sigoli, *J. Mater. Chem.*, 2012, **22**, 24109.
51 J. H. S. K. Monteiro, A. L. B. Formiga and F. A. Sigoli, *J. Lumin.*, 2014, **154**, 22.
52 R. A. Sá Ferreira, S. S. Nobre, C. M. Granadeiro, H. I. S. Nogueira, L. D. Carlos and O. L. Malta, *J. Lumin.*, 2006, **121**, 561.
53 G. V. Prakash and R. Jagannathan, *Spectrochim. Acta, Part A*, 1999, **55**, 1799.